ADVANCED ELECTRONIC MATERIALS
Open Access
www.advelectronicmat.de

Check for updates

Reliable Memristive Switching Empowered by Ag/NiO/W ReRAM Configuration for Multi-Level Non-Volatile Memory Applications

*Manvendra Chauhan, Sumit Choudhary, and Satinder K. Sharma**

Resistive random-access memories (ReRAM) are promising candidates for next-generation non-volatile memory, logic components, and bioinspired neuromorphic computing applications. The analog resistive switching (RS) tuning with a sizable memory window is crucial for realizing multi-level storage devices. This work demonstrates the multi-level storage capability of fabricated Ag/NiO/W ReRAM architecture, controlled through voltage modulations. The fabricated ReRAM structures exhibit stable bipolar analog RS, non-overlapping resistance, and endurance of ≈10^4 cycles, respectively, with marginal statistical variations/fluctuations. Also, the fabricated ReRAM offers highly controlled and stable retention characteristics tested up to ≈10^4 s with significantly controlled statistical variations/fluctuations. Adjacent thereto, it offers a substantially lower operating SET and RESET voltage of 1 and −1 V, respectively. Moreover, the non-overlapping multiple resistive states are observed with the voltage pulse modulation schemes. Furthermore, the current switching mechanism is described using a model proposed for the conductive filament growth and the contribution of the NiO/W interface layer (IL) toward notable RS of fabricated Ag/NiO/W structures.

1. Introduction

To further downscale next-generation memory devices, a paradigm change from charge-based to resistance-based memories has become necessary.[1] Due to quick operational speed, facile device structure, ease of materials integration, and dependability, resistive switching (RS) random-access memories (ReRAM) have garnered a lot of attention among resistance-based memory devices.[2–5] Although the RS mechanism has been broadly researched, including localized conducting filaments[6–8] and area-dependent interfacial energy barrier modulation,[2,9,10] reliability difficulties, such as operational parameter dispersion and resistance state fluctuation, have not significantly improved. It is widely known that filament critical concerns, including an abrupt current overshoot and reliability issues, can arise from local temperature upsurge and self-heating effects in the filament region.[11]

ReRAM-based non-volatile memories have been reported to mimic neuron bodies similar to the human brain by emulating Ca^{+} and Na^{+} with the ion/cation movements across the switching layer (SL).[12] Enabling synaptic functionality through hysteric memristive behavior caused by ions/cations migration across the SL from the top electrode (TE) to the bottom electrode (BE) is one of the most attractive features of ReRAM. Another valuable aspect of ReRAM devices is their ability to enforce multi-level resistance operations[13] that facilitate multiple discrete synaptic weights.[14] These characteristics of ReRAM vastly motivate the researchers to exploit various transition metal oxides by incorporating them into distinctive ReRAM configurations (Table S2, Supporting Information, highlights the neuromorphic applications of various metal oxides used as switching layers in the ReRAM architecture, discussed under Section S2, Supporting Information).

Various transition metal oxides, such as HfO_2, ZrO_2, NiO, ZnO, and WO_3, have been utilized as either SL or buffer/ ILs in ReRAM devices.[15–17] NiO, a transition metal oxide, has a semiconducting phase and a significant thermal conductivity of ≈49 W mK^{-1}.[18] These characteristics help to reduce the effects of local heating and enhance the controllability of conductive filaments (CF). Several NiO-based ReRAMs have been reported but are unappealing because of their insignificant endurance (<10^3), small switching window, or low resistance ratio (RR).[16,17,19–21] More tangibly, the stochastic nature of ReRAM devices, which rely on the minute movement of charged carriers, is the primary cause of these reliability problems.[22–24] The selection of metals as TEs or BEs plays a crucial role in improving the switching kinetics of ReRAM devices. Due to the tight correlation between SL and metal electrodes, any electrical parameter that modifies the device's performance must be compatible with the electrodes and the oxide's electrochemical characteristics; for instance, Ag

M. Chauhan, S. Choudhary, S. K. Sharma
School of Computing & Electrical Engineering (SCEE)
Indian Institute of Technology (IIT)
Mandi, Himachal Pradesh 175005, India
E-mail: satinder@iitmandi.ac.in

The ORCID identification number(s) for the author(s) of this article can be found under https://doi.org/10.1002/aelm.202300724

© 2024 The Authors. Advanced Electronic Materials published by Wiley-VCH GmbH. This is an open access article under the terms of the Creative Commons Attribution License, which permits use, distribution and reproduction in any medium, provided the original work is properly cited.

DOI: 10.1002/aelm.202300724

or Cu as TE has been utilized for ReRAM TE/SL/BE stack, where most of the cases cation (Ag^+ or Cu^+) migration involves in the electroforming process, that manifest the resistive switching effect in the ReRAM. Also, diffusion of these cations is considered to be essential for neuromorphic memory designs as it emulates the ionic flow (Ca^{2+}, Mg^{2+}, and Na^+) dynamics of bio-synapse.[25] Such ReRAM configurations, well established as electrochemical metallization (ECM) memories utilized inert (BEs), such as Pt, demonstrating discrete/digital switchings of low resistance state (LRS) and High resistance state (HRS). ECM memories mainly suffer aberrant resistance values due to large current variations during consecutive switching cycles and retention operations. Material engineering, for instance, doping in the SL,[26] IL modification,[27] and electrically inducing oxide interface between electrode and SL[28–33] is one of the few approaches employed from a macroscopic control perspective to obtain a precisely desired resistance state and switching control. The latter interface engineering is achieved through utilizing oxidizable metals (e.g., W Al, Hf, and Ti) as one of the electrodes in the metal-insulator-metal (MIM) stack of ReRAM. Particularly, it has been demonstrated that the selection of oxidizable electrodes at the interface has significantly controlled the filament growth by exchange of ions/cations at the BE interface and hence improved the switching performance of ReRAMs.[34]

The selection of an oxidizable metal electrode is governed by Gibb's free energy of the electrode, diminishing the requirement of additional oxide IL (stopping layer). The Gibbs free energy (ΔG_f), which measures the oxidation stability/instability of metals, can also be used to assess the reactivity of the various oxidizable electrodes with the oxide interface.[35] C. B Lee et al. also discussed the significance of free energy for the oxidation of metal as a selection criterion for TEs or BEs to control the high/low resistance state (HRS)/(LRS), as well as the endurance characteristic of ReRAM.[30] Additionally as aforementioned, by incorporating oxidizable metal electrodes, such as W, into the MIM stack of ReRAM, an IL between the metal and oxide is electrically induced, diminishing the requirement of additional oxide IL (used as an oxygen reservoir or stopping layer) over the oxide SL with the primary goal of improving ReRAM device endurance. Also, the metal W is a popular choice of material in many back ends of the line (BEoL) procedures for vertical interconnected access (VIA) across neighboring layers in the metal stacks.

Hence, in this work, we have incorporated oxidizable metal "W" as BE in the ECM ReRAM configuration, where NiO SL is sandwiched between Ag (TE) and W (BE). Further, we discussed the possibility of the formation of oxide IL w.r.t NiO SL at Ag/NiO and NiO/W interface using pseudo ternary phase diagrams prior to investigating the resistive switching behavior of Ag/NiO/W. The results demonstrate that the fabricated Ag/NiO/W ReRAM structures exhibit forming-free, analog switching behavior supported by ohmic and trap-controlled space charge limited conduction (TC-SCLC) model. In addition, it shows multi-level RS and resistance states controlled by modulating the voltage from −1 to −3 V. Also, to further establish the scientific relevance of the choice of electrode materials with respect to the NiO SL, we have fabricated and tested three more sets of ReRAM configurations: i) Ag/NiO/Pt (conventional ECM configuration), ii) Pt/NiO/W (asymmetrical electrode valence change memory (VCM) configuration), and iii) W/NiO/W (symmetrical electrode VCM configuration) (discussed under Sections S3 and S4, Supporting Information). Moreover, this work also provides a point of view on the selection of metal electrodes w.r.t the material utilized as SL.

1.1. Electrode Selection Criteria

The thermodynamic stability of the electrode must be considered forehand for a metal to be considered for integration onto metal oxide-based MIM stack for ReRAM applications. The criterion of metal incorporated as a TE and BE primary is based on work functions and the tendency to form Schottky or ohmic contact with the SL.[36] It has already been reported that the dependence of RS over metal electrodes is not solely developing from the work function or by the metal electrode's interaction with SL oxide but rather is a result of Gibb's free energy for oxidation of metal (used as TE/BE) compared to SL oxidation.[30] Here, the thermodynamic stability of the metal electrode with respect to the reaction with NiO and the tendency of formation of interface oxide layer between NiO and metal electrode contacts can be anticipated through a pseudo ternary phase diagram,[37,38] as shown in **Figure 1**.

Figure 1a shows a broken tie line exists between NiO and Ag_2O that predicts the phases in contact with one another are possibly unstable, whereas the Gibbs free energy (ΔG_f) for formation of Ag_2O (−11.06 kJ mol^{-1}) is lower than that of NiO (−211.364 kJ mol^{-1}) that depicts the low probability of silver oxide (AgO_y) phase formation, but Ag is highly diffusive in semiconducting oxides due to their high diffusion constant, that is, $D = D_O \exp(-Q/KT)$.[30] Hence, Ag metal certainly contributes to the CF formation by Ag^+ movement across NiO SL.

Meanwhile, a continuous tie line between NiO and W in Figure 1b implies the formation of stable tungsten oxide (WO_y) IL at the NiO/W interface owing to ΔG_f for tungsten oxide phases, such as WO_2, $WO_{2.72}$, $WO_{2.90}$ and WO_3, respectively, are −533.51, −708.17, −743.04, and −763.56 kJ mol^{-1},[39] which are significantly higher than ΔG_f for NiO, facilitate the formation of oxide IL between NiO/W as ΔG_f becomes more negative, the corresponding metals oxygen affinity rises, which implies that the oxide formation is favorable and thermodynamically stable.[37] The values for Gibbs free energy (ΔG_f) for particular oxide phases are shown in Figure 1c. Moreover, the pseudo phase diagrams expound the higher thermal stability of WO_y with respect to the NiO SL, which critically influences the endurance property of NiO-ReRAM.

2. Results and Discussion

The fabricated Ag/NiO/W ReRAM device structures have shown forming-free bipolar and stable analog resistive switching cycles. The RS characteristics of the Ag/NiO/W ReRAM structure are shown in **Figure 2**. The memory behavior of the ReRAM device with cyclic voltage loops of −1 V to 0 to +1 V to 0 and finally to −1 V is shown in Figure 2a. Interestingly, significant, reliable RS characteristics were observed. The pristine device was initially conducted in the HRS. The SET process occurs when the voltage sweeps from 0 to +1 V, the current gradually rises to 3.97 A cm^{-2} to meet the self-compliance at 0.93 V and further tends toward saturation at 1 V, which we consider as SET voltage (V_S) for

© 2024 The Authors. Advanced Electronic Materials published by Wiley-VCH GmbH
2199160x, 0, Downloaded from https://onlinelibrary.wiley.com/doi/10.1002/aelm.202300724 by Indian Institute Of Technology Mandi, Wiley Online Library on [22/01/2024]. See the Terms and Conditions (https://onlinelibrary.wiley.com/terms-and-conditions) on Wiley Online Library for rules of use; OA articles are governed by the applicable Creative Commons License

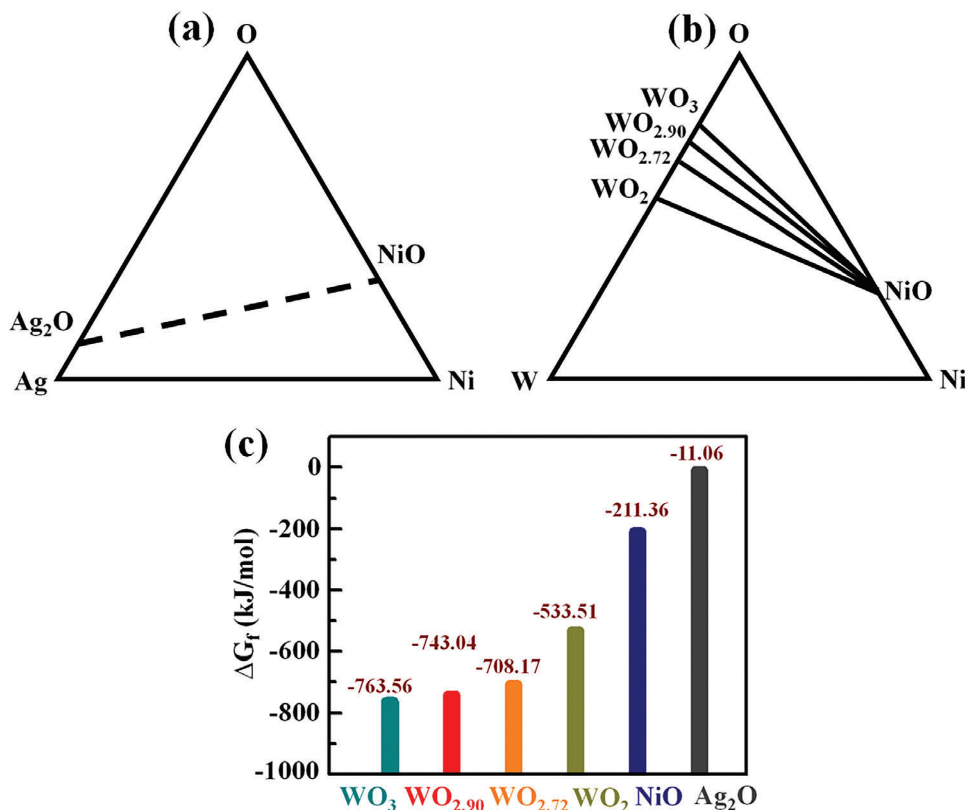

Figure 1. The pseudo ternary phase diagrams predicting the thermal stability of a) Ag/Ni/O, b) W/Ni/O at 300 K, and c) Gibb's free energy of metal oxides.[39]

analog switching of the fabricated Ag/NiO/W ReRAM structures. When the voltage sweeps to the negative region at RESET voltage (V_R) −1 V, the device again slowly RESET to the HRS. These gradual current transitions between SET and RESET operations are termed, analog switching, which is crucial for the emulation of neural development. To be effectively utilized as synapses in neuromorphic computing, the devices must show analog RS to mimic the incremental variation of the synaptic weight.[40]

Notably, Ag/NiO/W ReRAM delivers ≈10^4 consecutive bipolar RS cycles durability, as depicted in Figure 2b. Such high durability offered by ReRAM devices attributed to the WO_y IL induced at the NiO/W interface that provided a barrier layer facilitating the confined growth of metallic filament reaching toward BE. In addition, the induced WO_y IL acts as a series resistive path in determining the abrupt change in current in contrast to the variation in the voltage that attributes the gradual increment/decrement of conduction current during switching.

I–V curve presented in Figure 2a is plotted again in the double-logarithm (log-log) scale and linearly fitted at positive polarity as shown in Figure 2c, where the devices reached to SET state to elucidate the conduction mechanism of the Ag/NiO/W ReRAM devices. The slope at a lower voltage where the ReRAM device is in or reaching HRS is ≈1 (Ohmic conduction), while it displayed a slope of log-log *I–V* curve at higher voltages (>0.22 V) during SET process ≈6, respectively, that suggests a strong TC-SCLC switching in ReRAM. The TC-SCLC model[41] observed in log*I*–log*V* curves during the LRS cycle of each device validate the existence of an ohmic region ($I \alpha V$) and child's law region ($I \alpha V^2$) that suggests the ion/cation movement across the NiO SL.

To further examine the reliability, stability, and uniformity of Ag/NiO/W ReRAM devices, the DC endurance cycle versus resistance graph was plotted at a read voltage of 0.3 V as shown in Figure 2d. The RR is maintained at ≈52 up to 10^4 RS cycles. This confirmed the fabricated ReRAM switching from HRS to LRS exhibiting at least one level in memory operation.

2.1. Multi-Level Controlled Resistive Switching of Ag/NiO/W ReRAM Device

The Ag/NiO/W ReRAM device incorporating oxidizable BE maintained its current conduction and switching *I–V* characteristics up to 10^4 cycles, as shown in Figure 2d. Further investigations were performed to check the reliable multi-level RS behavior of the ReRAM devices. The multi-level controlled switching characteristics of Ag/NiO/W ReRAMs are presented in **Figure 3**. Here, the multi-level RS is obtained by applying voltage level modulations, resulting in multiple resistance states. As shown in Figure 3a, for the inspection of the multiple resistance states, the device directed through modulating V_p (max) from +3 to +1 V and V_n (max) from −3 to −1 V. Five voltage switching (V_p and V_n) levels were examined with five different voltage cycles applied in dual sweep mode. In the first cycle of V_p (max) = +1 V and V_n (max) = −1 V, the Ag/NiO/W ReRAM device repeats the

© 2024 The Authors. Advanced Electronic Materials published by Wiley-VCH GmbH

2199160x, 0, Downloaded from https://onlinelibrary.wiley.com/doi/10.1002/aelm.202300724 by Indian Institute Of Technology Mandi, Wiley Online Library on [22/01/2024]. See the Terms and Conditions (https://onlinelibrary.wiley.com/terms-and-conditions) on Wiley Online Library for rules of use; OA articles are governed by the applicable Creative Commons License

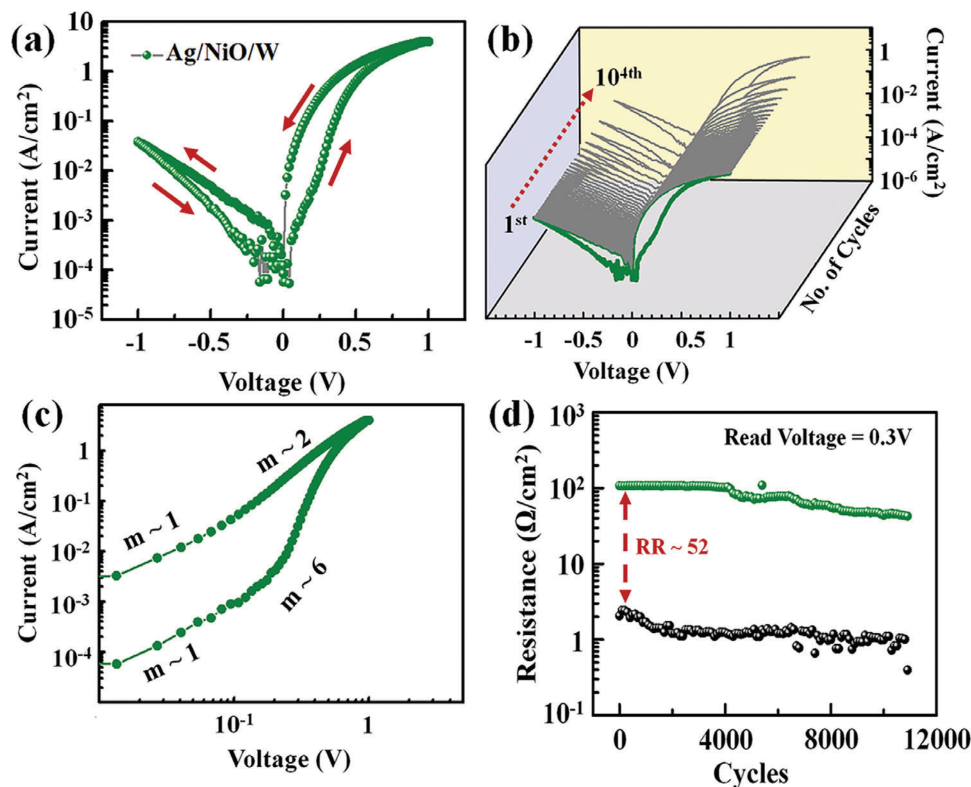

Figure 2. The RS Characteristics of a) Ag/NiO/W ReRAM device with voltage loops of –V to 0 to V to 0 to –V. b) A waterfall plot showing ≈10^4 resistive cycles of fabricated Ag/NiO/W ReRAM, c) the double logarithm characteristics of Ag/NiO/W ReRAM device in LRS, and d) DC endurance cycles of Ag/NiO/W ReRAM device tested at 0.3 V read voltage.

same behavior as shown in Figure 2a. During LRS, it reached up to 3.97 A cm^{-2} and met the self-compliance at 0.93 V, tending toward saturation at 1 V, while at HRS, the current decays gradually from 0.036 to $\approx 1.37 \times 10^{-4}$ A cm^{-2}. In contrast, the second switching cycle for another V_p (max) and V_n (max) values of +2 and −2 V, respectively, maintained the same LRS conduction state; however, during HRS operation, it decays gradually from 0.45 to $\approx 7.57 \times 10^{-5}$ A cm^{-2}. Again, the third level of the switching cycle was executed at V_p (max) = +3 V and V_n (max) = −3 V, which displayed the distinctively highest current level of 1.98 A cm^{-2} at HRS, which apparently gradually decays to the $\approx 7.89 \times 10^{-4}$ A cm^{-2}; meanwhile, the LRS current showed the same current value as of previous two levels of RS operations. From these three distinct switching levels of operation, it can be observed that the HRS current value is changing only with the V_n (max). The current value during LRS remains constant. Such current conduction of RS affirms that the resistance states of Ag/NiO/W ReRAM structures vary with the variation in the V_n (max) excitations, which also agrees with the previously reported multi-storage ReRAMs.[19,42,43] Further, while exploring another switching level below ± 1 V, V_p (max) and V_n (max) are respectively set to 0.5 and −0.5 V, resulting in inadequate RS behavior as depicted in Figure 3a, which was imprudent for further ReRAM analysis. The measured LRS current at V_p (max) = 0.5 V was not maintained at the same value as was observed in the aforesaid-investigated RS levels. To further extend the reliability investigation of the multi-level RS of the device, we increased the biasing as V_p (max) = 4 V and V_n (max) = −4 V; the current conduction increased up to the set compliance current of 100 mA, and no RS was observed in this case as shown in inset Figure 3a.

In order to elucidate the competency of Ag/NiO/W ReRAM structures for multi-level storage applications, Figures 3b and 3c demonstrate the retention and endurance properties, respectively. The retention test was performed for Ag/NiO/W ReRAM, by RESET the device initially at a voltage of −1 V (HRS-1), and then read-out operations were performed at a low read voltage of 0.3 V, up to 10^4 s. The proposed ReRAM retains its resistance state HRS-1 with negligible fluctuations while reaching 10^{4th} s. Similarly, retention for HRS-2 and HRS-3 was plotted at 0.3 V by resetting the device at −2 and −3 V, respectively. For both cases, the retention was considerably better than the HRS-1 and no significant degradations were observed. Meanwhile, the LRS current density of Ag/NiO/W ReRAM structures at voltages of 1, 2, and 3 V were the same, that is, 3.97 A cm^{-2}, as shown in Figure 3d, which was plotted from the LRS current values of Figure 3a and HRS levels at −1, −2, and −3 V modulation as shown in Figure 3d inset, shows that the HRS varies with increase in negative polarity. Therefore, retention of the device structures at LRS was tested at the same read voltage of 0.3 V by SET the device at 1 V because the device meets the same current compliance at 2 and 3 V itself during SET operations, whereas the three distinctive HRS retentions were performed to examine the multi-level storage controllability by maximum stop voltage, that is, V_n (max) modulations. Figure 3b shows a quite reliable retention

© 2024 The Authors. Advanced Electronic Materials published by Wiley-VCH GmbH

2199160x, 0, Downloaded from https://onlinelibrary.wiley.com/doi/10.1002/aelm.202300724 by Indian Institute Of Technology Mandi, Wiley Online Library on [22/01/2024]. See the Terms and Conditions (https://onlinelibrary.wiley.com/terms-and-conditions) on Wiley Online Library for rules of use; OA articles are governed by the applicable Creative Commons License

2199160x, 0, Downloaded from https://onlinelibrary.wiley.com/doi/10.1002/aelm.202300724 by Indian Institute Of Technology Mandi, Wiley Online Library on [22/01/2024]. See the Terms and Conditions (https://onlinelibrary.wiley.com/terms-and-conditions) on Wiley Online Library for rules of use; OA articles are governed by the applicable Creative Commons License

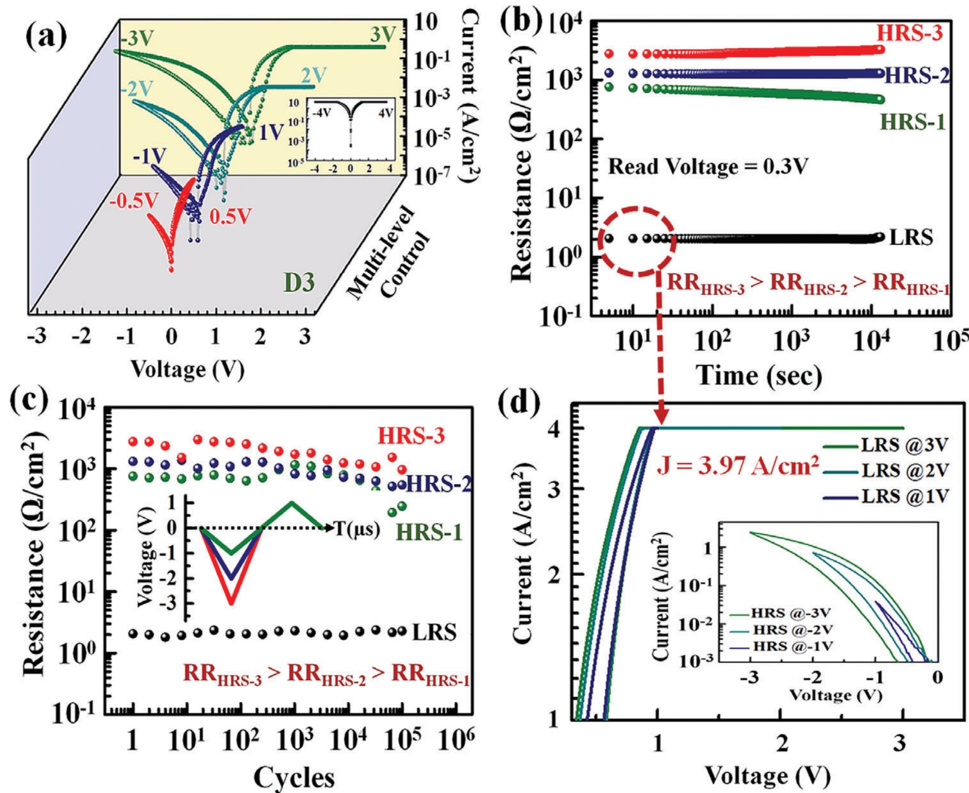

Figure 3. a) Multi-level controlled resistive switching characteristics of Ag/NiO/W ReRAM device (inset: *I–V* characteristic of Ag/NiO/W ReRAM for −4 to 4 V dual sweep). b) Multi-level retention data taken for three different HRS and an LRS. c) Endurance of the multi-level resistance states of Ag/NiO/W at room temperature (inset: applied voltage pulse) and d) LRS current levels at V_S = 1, 2, and 3 V (inset: HRS current levels at V_R = −1, −2, and −3 V).

for Ag/NiO/W ReRAM structures with significantly lower fluctuations, which were later authenticated through statistical variability in **Figure** 4d and also, it is in agreement with the previous reports on ReRAM devices.[42,44,45]

Here, the storage levels that are HRS-1, HRS-2, and HRS-3 obtained by modulating maximum stop voltages V_n (max) as −1, −2, and −3 V, respectively. Irrespective of variation in the voltages from 1 to 3 V, the similar LRS current density was measured for all the tests because the device meets the current compliance at 1 V itself, as presented in the *I–V* plot for LRS in Figure 3d. In all the cases, the pulse of width = 10 µs, rise/fall time = 100 µs, and delay time = 100 µs was applied for the endurance testing with the pulse amplitudes of −1, −2, and −3 V for HRS, and 1 V for LRS as shown in Figure 3c inset. To this extent, from Figure 3c, a significant variation in the resistance of Ag/NiO/W ReRAM can be observed: $RR_{HRS\text{-}3}$ ($\approx 1.34 \times 10^3$) > $RR_{HRS\text{-}2}$ ($\approx 6.36 \times 10^2$) > $RR_{HRS\text{-}1}$ ($\approx 3.68 \times 10^2$), which is in line with the previous reports.[19,42,43] Here, $RR_{HRS\text{-}1}$, $RR_{HRS\text{-}2}$, and $RR_{HRS\text{-}3}$ represent the resistance ratio w.r.t the voltage modulations of −1, −2, and −3 V, respectively, where RR denotes the resistance ratio between HRS and LRS levels. In this manner, the fabricated Ag/NiO/W ReRAM exhibits three more distinct levels to operate while switching from LRS to HRS by modulating voltages as V_n (max) as −1, −2, and −3 V, and V_p (max) = 1 V. Such noteworthy switching behavior indicates the multi-level storage capability of fabricated Ag/NiO/W ReRAM devices in the next-generation computing systems. Therefore, the Ag/NiO/W ReRAM exhibits multi-level controlled switching reliable characteristics by controlling V_n (max) from −1 to −3 V, which is a vital aspect of high-density storage applications.

Moreover, the reliability of multi-level endurance and retention tested for Ag/NiO/W ReRAM structures is shown in Figure 4. The cumulative distribution extracted from endurance cycles and retention data is shown in Figures 4a,c, respectively, demonstrating a well-separated and uniform distribution of each resistance state (i.e., LRS, HRS-1, HRS-2, and HRS-3). The statistical variability (σ/μ) shown in Figures 4b,d, calculated from the cycle-to-cycle endurance data and the retention data, respectively; where σ is the standard deviation, and μ is the mean obtained for each resistance state (LRS, HRS-1, HRS-2, and HRS-3). The plotted statistical variability shown in Figure 4b displays considerably small variation percentages for each resistance state, that is, 7.5% for LRS, 34.3% for HRS-1, 29.1 for HRS-2, and 30.2% for HRS-3. It can be observed that the slightest variation of 7.5% observed at LRS is attributed to a formed controlled, confined, and stable conducting filament resulting in stable and uniform current conduction.[42] Additionally, the statistical variability (σ/μ) versus resistance states plot shown in Figure 4d, measured from retention data, presented σ/μ (%) for each resistive state as 2.4% for LRS, 7.8% for HRS-1, 2.8% for HRS-2, and 3.9% for HRS-3. Such significantly minimal variations predict no overlapping of consecutive states and maintain an almost constant resistance ratio. This effect, which has also been noted for Ag TE devices,[46] is especially beneficial for the application of improving the multi-bit storage capabilities.

© 2024 The Authors. Advanced Electronic Materials published by Wiley-VCH GmbH

2199160x, 0, Downloaded from https://onlinelibrary.wiley.com/doi/10.1002/aelm.202300724 by Indian Institute Of Technology Mandi, Wiley Online Library on [22/01/2024]. See the Terms and Conditions (https://onlinelibrary.wiley.com/terms-and-conditions) on Wiley Online Library for rules of use; OA articles are governed by the applicable Creative Commons License

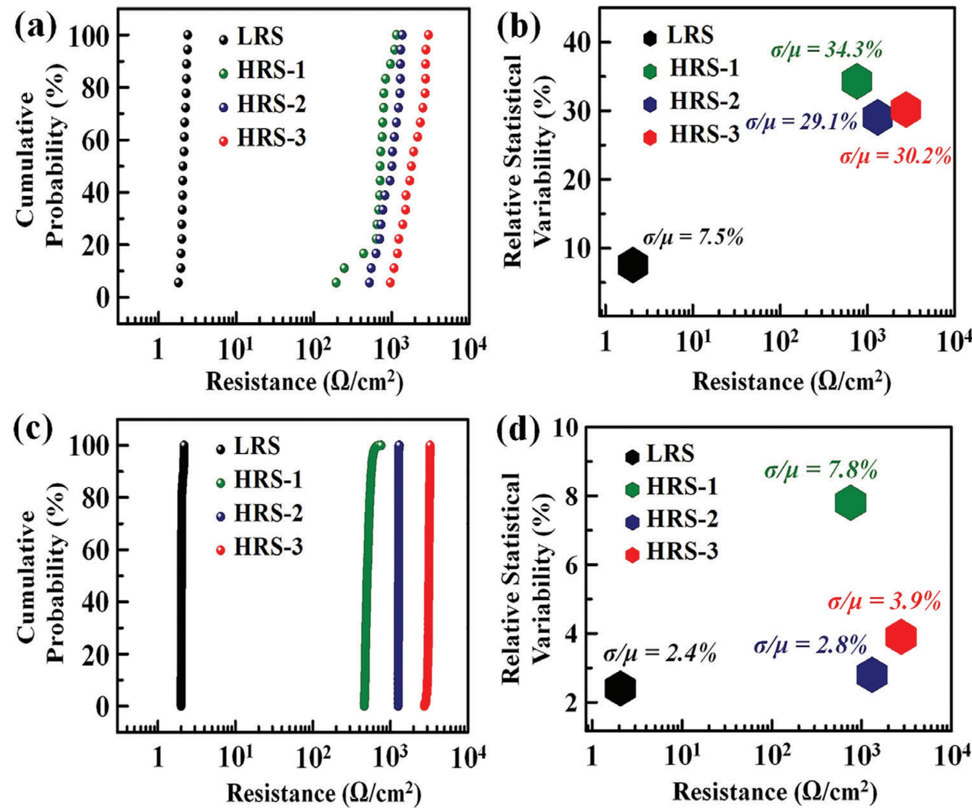

Figure 4. a) Cycle-to-cycle cumulative distribution of four resistance states, b) relative statistical variability for four resistant states calculated for endurance data, c) cumulative distribution of four resistance states obtained for retention data, and f) relative statistical variability for four resistance states calculated for retention data.

2.2. RS Mechanism of the Ag/NiO/W ReRAM Device

Considering bipolar I–V characteristics from Figure 2a, it can be estimated that the HRS conduction during negative voltage sweep is due to the Schottky emission. The reset state for Ag/NiO/W ReRAM suggests the formation of Schottky contact at the Ag/NiO interface or NiO/W interface. Since, in the proposed ReRAM device structures, TE is Ag (ϕ_m = 4.26 eV; ϕ_m = work function),[47] which is highly diffusive in semiconducting oxides.[30,48,49] Hence, herein, **Figure 5**b shows that the Ag atoms diffused at the Ag/NiO interface. Hence, considering this diffusivity of Ag into the SL interface, we assume that the Schottky barrier at Ag/NiO will diminish or the contact become pseudo-ohmic. Therefore, considering only W (ϕ_m = 4.55 eV)[47] forming Schottky contact with NiO (ϕ_m = 5.3 eV)[50] SL resulting in the transition from LRS to HRS[51] as it qualifies the Schottky condition, $\phi_m < \phi_s$. Moreover, the reported work[52] on nickel oxide-based Schottky diodes demonstrated the Richardson plot at different temperatures and concluded that the thermionic emission will dominate at low voltage. Also, the various reports demonstrated modified equations and fitting analysis to extract the Schottky barrier at the metal/oxide interface when thermionic emission dominates at room temperature.[51,53,54] Considering this, to clarify the dependence of current in the HRS on the negative sweep voltage, we have extracted the Schottky barrier height at a reverse voltage (i.e., negative polarity) by plotting the current density in natural log (ln) as a function of the square root (SQRT) of the negative sweep voltages (Figure 5a).

The Schottky barrier height was estimated at a smaller voltage (< −0.5 V) and at room temperature ($T \approx 300$ K) as shown in Figure 5a, with the following current–voltage relation[51]

$$J = (A^*) \times T^2 \times \exp\left(\frac{\frac{q\sqrt{qE}}{4\pi\varepsilon_i}}{kT} - -\frac{q\phi_{BE}}{kT}\right) \tag{1}$$

The linear fitting of ln(J) versus $V^{1/2}$ plot demonstrates that the current density is proportional to the SQRT of applied negative voltage sweep, implying that the current flow in the HRS was delimited by Schottky emission, that is, Equation (1), where J is current density, A^* is the Richardson constant which is 96 A cm^{-2} K^{-2} for NiO,[55] E is the electric field, ϵ_i is the dynamic permittivity, η is the ideality factor, k is the Boltzmann constant, T is the absolute temperature, q is electric charge, and ϕ_{BE} is the Schottky barrier height at NiO/W interface which then extracted as 0.689 eV, from $\phi_{BE} = kTln(A^* \times \frac{T^2}{J_O})/q$ relation, where reverse saturation current (J_O) obtained from the intercept as J_O = exp (intercept) = exp (−10.53) ≈ 2.26 e-5 A cm^{-2}.

A proposed resistive switching mechanism model is illustrated in Figure 5. When W is employed as BE in TE/NiO/BE ReRAM structures, the oxygen exchange reaction occurs between NiO SL

 © 2024 The Authors. Advanced Electronic Materials published by Wiley-VCH GmbH

ADVANCED ELECTRONIC MATERIALS Open Access
www.advelectronicmat.de

Figure 5. a) ln(*J*) versus SQRT(*V*) plot to extract Schottky barrier height corresponding to the NiO/W contact. b–f) Illustration of the proposed resistive switching mechanism for Ag/NiO/W ReRAM device structure containing interfacial layer at NiO/W.

and W (BE), which means oxygen extracted from NiO, oxidizes the oxidizable back electrode W to form WO_y at the interface as predicted through pseudo ternary phase diagram illustrated in Figure 1. This oxygen exchange reaction and the formation of oxide IL introduced oxygen vacancies (V_O) inside the SL, even in its pristine state, as shown in Figure 5b. When Ag is employed as TE in TE/NiO/W ReRAM structure, there might be a few amounts of Ag^+ cations diffuse around the Ag/NiO interface,[56–58] which affect the Schottky barrier (ϕ_{TE}) diminishing or pseudo-ohmic contact formation at the interface during pristine state of the device as depicted in Figure 5b.

After applying positive voltage within the range from 1 to 3 V, Ag/NiO/W became forward biased while BE is grounded, and the oxygen ions (O^{2-}) migrate from WO_y IL toward TE under a positive electric field that suppresses the stochastic distribution of V_O across NiO SL and limits the vacancy based CF growth. In this instance, the induced WO_y IL served the oxygen reservoir and suppressed the vacancy defect generation throughout the successive RS cycles. The primary process of V_O generation during CF forming is majorly due to intrinsic defect generation owing to oxygen expulsion from metal oxide as shown in Equation (2)[28]

$$2O^{2-} \leftrightarrow V_O + 2e^- + \frac{1}{2}O_2\,(g) \quad (2)$$

However, when the electrons are localized at the metal cations (M^+), then Equation (2) translates to Equation (3), which is also elaborated for Ag^+ cations in this discussion.

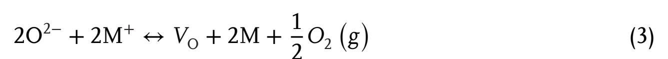

$$2O^{2-} + 2M^+ \leftrightarrow V_O + 2M + \frac{1}{2}O_2\,(g) \quad (3)$$

The migration of O^{2-} from WO_y IL leads to the generation of V_O at the NiO/W interface, which results in the Schottky barrier (ϕ_{BE}) lowering at W (BE),[59,60] where subsequently, under positive biasing, Ag atoms diffused from TE starts ionizing as $Ag \rightarrow Ag^+ + e^-$, and the Ag^+ moved across NiO SL to reach at BE. However, O^{2-} ions from WO_y IL also migrated subsequently toward the NiO SL as $O_2 \rightarrow O^{2-} + 2e^-$and due to the

© 2024 The Authors. Advanced Electronic Materials published by Wiley-VCH GmbH

2199160x, 0, Downloaded from https://onlinelibrary.wiley.com/doi/10.1002/aelm.202300724 by Indian Institute Of Technology Mandi, Wiley Online Library on [22/01/2024]. See the Terms and Conditions (https://onlinelibrary.wiley.com/terms-and-conditions) on Wiley Online Library for rules of use; OA articles are governed by the applicable Creative Commons License

electrons exchange, Ag^+ reduced to the Ag atoms in proximity at the grounded W (BE) as $Ag^+ + e^- \rightarrow Ag$. The formation of metal filament and Ag^+ drift through the SL consequently reduced the resistivity of SL.[34,59] Since the Ag^+ can rapidly drift across SL but it is restricted near WO_y IL due to the electron exchange reaction as aforementioned and thus starts reducing to Ag atom near IL after receiving electron, consequently forming a confine CF (responsible for controlled switching with minimum fluctuations and noise during endurance and retention tests) across the IL reaching to BE as shown in Figure 5c. This process instigated the resistive switching during positive voltage sweep and thus, resulted in the LRS current density of ≈3.97 A cm^{-2}. Here, the current density was the same for each positive voltage, that is, 1, 2, and 3 V, which concludes the existence of reliable & stable metallic CF formation, which does not alter under the applied voltage range of 1–3 V.

Meanwhile in the negative voltage sweep, when −1 V was applied at Ag (TE), the O^{2-} ions migrated toward the WO_y IL and filled the V_O inside the IL that modulates the ϕ_{BE} where W (BE) and SL interface get reversed biased. Consequently, the Ag atoms forming CF oxidized to Ag^+ cations, which then attracted back toward Ag (TE) under a negative electric field and got reduced to Ag atoms at TE. This process leads to the rupture of CF, leaving a CF gap in the WO_y IL, thus the HRS current decreased as shown in Figure 5d. As the negative voltage applied at Ag (TE) increased to −2 V, more Ag atoms from CF oxidized to Ag^+ cations, resulting in an increment in the CF gap inside the NiO SL and the electrons transverse from the oxidation of Ag atoms traveled toward the W (BE) through hopping mechanism as shown in Figure 5e, results in the LRS current level increment in the negative polarity in comparison to the case for −1 V applied at TE. Similarly, when TE biased with −3 V, the CF gap increased and more electrons hopped toward BE (Figure 5f) as more Ag atoms from the CF oxidized to Ag^+. The increment in the CF gap with the increasing voltage at negative polarity (from −1 to −3 V) is responsible for $RR_{HRS\text{-}3}$ (≈1.34×10^3) > $RR_{HRS\text{-}2}$ (≈6.36×10^2) > $RR_{HRS\text{-}1}$ (≈3.68×10^2) as shown in Figure 3b,c. Though the CF gap increased with the negative voltage, the increment in the LRS current level was observed at −3 V. This was attributed to the release of excess electrons inside the SL during Ag oxidation that traveled through WO_y IL to BE and was consequently responsible for the rise in the leakage current at reverse bias. Therefore, in the multi-level bipolar *I–V* switching characteristics at different RESET voltages, shown in Figure 3a, the rise in the LRS current levels at negative polarity might be attributed to the excess negative charge carriers hopping toward BE, which increases with the increment in the negative voltage applied at Ag (TE) that results in higher leakage current at the higher negative voltages (V_R) (less than the breakdown voltage for SL). However, while modulating voltages from −1 to −3 V, the current density at the negative polarity remains lower than that attained at the positive polarity due to the Schottky effect as shown at the SL/BE interface during negative voltage sweeping.

The gradual variation in current conduction toward HRS suggests the partial rupture of metallic CF filament and the presence of intrinsic defect density inside the NiO SL. These defects will again filled at SET operation owing to O^{2-} migration from WO_y IL and the process will continue with SET and RESET operations. The aforementioned RS mechanism model for fabricated Ag/NiO/W ReRAM structures suggested that the formation and rupture of metallic filament responsible for the resistive switching and illustrate the RS behavior of the device at V_p (max) and V_n (max) ranging from ± 1, ± 2, and ± 3 V. Here, V_p (max) and V_n (max) are referred to the maximum stop voltage for positive and negative polarities, respectively.

Similar reports on self-rectifying ReRAM devices incorporating active metals (Ag or cu) also suggest the presence of conducting filament across the switching layer.[46,49,61] Also, the diffusivity of Ag across the switching layer under the electric field must not be neglected.[30,40,46,49,57] Hence, the demonstrated switching mechanism of Ag/NiO/W ReRAM structures presented the formation and rupture of conducting filament with the modulation in the Schottky barrier at the NiO/W interface.

When the ReRAM was swept with a −4 to 4 V potential loop, the substantial current conduction was observed at −4 V which indicates the device was initially at LRS which entails the presence of a conducting channel between the TE and BE. This conducting channel might be of oxygen vacancy (V_O) filament, formed due to significant O^{2-} migration across SL toward BE at such a high electric field induced at −4 V. While reaching +4 V, the device continued to operate in its LRS current level due to Ag CF formed at positive polarity as discussed above. Thus, due to the presence of hybrid filament (V_O CF at negative polarity and Ag CF at positive polarity), the fabricated Ag/NiO/W showed hysterisis-free symmetrical *I–V* characteristics as shown in Figure 3a inset. The permanent presence of filament across the SL enforces the device to remain at the LRS level without switching to HRS.

In order to further investigate the oxide IL formation at Ag/NiO and NiO/W interfaces, an XPS depth profile was performed, followed by the surface etching at 1 KeV, Ar^+ ion plasma. The elementary trace analysis were performed by XPS data collection followed by etch cycles until the interface of interest and BE was approached, as shown in **Figure 6**a.

The chemical stability of the Ag/NiO interface (Figure 6b) was analyzed using the core/valence spectrum of Ag and O_2 to examine the possibility of the formation of silver oxide at the interface. The peak obtained at 368.12 and 374.18 eV represents Ag3*d*5/2 and Ag3*d*3/2, respectively. These Ag3*d* peaks are symmetrically spread and relative to the Ag(0) orbits representing metallic silver,[60] which also resonates in the Ag/NiO/W RS mechanism discussed in Section 2.2, where it is stated that the Ag will diffuse through Ag/NiO interface and contributes in the formation of metallic CF, without forming any oxide IL. However, the interpretation of XPS spectra for W4*f* analyzed at the NiO/W interface was deconvoluted to four peaks at 32.1, 33.3, 35.9, and 37.9 eV, respectively, presenting W4*f*7/2, W4*f*5/2, W4*f*7/2, and W4*f*5/2[61] as shown in Figure 6c. Here, two asymmetrical peaks at 35.9 and 37.9 eV suggest that the W oxidized at the NiO/W interface represents a high population of W^{6+} oxidation states, which is relative to the formation of tungsten trioxide, that is, WO_3.

Hence, this XPS analysis performed at NiO/W interfaces confirms the presence of a tungsten trioxide layer at the NiO/W interface, which has already been predicted in Figure 1, additionally its contribution in Ag/NiO/W RS has also been discussed in Section 2.2.

© 2024 The Authors. Advanced Electronic Materials published by Wiley-VCH GmbH

2199160x, 0, Downloaded from https://onlinelibrary.wiley.com/doi/10.1002/aelm.202300724 by Indian Institute Of Technology Mandi, Wiley Online Library on [22/01/2024]. See the Terms and Conditions (https://onlinelibrary.wiley.com/terms-and-conditions) on Wiley Online Library for rules of use; OA articles are governed by the applicable Creative Commons License

2199160x, 0, Downloaded from https://onlinelibrary.wiley.com/doi/10.1002/aelm.202300724 by Indian Institute Of Technology Mandi, Wiley Online Library on [22/01/2024]. See the Terms and Conditions (https://onlinelibrary.wiley.com/terms-and-conditions) on Wiley Online Library for rules of use; OA articles are governed by the applicable Creative Commons License

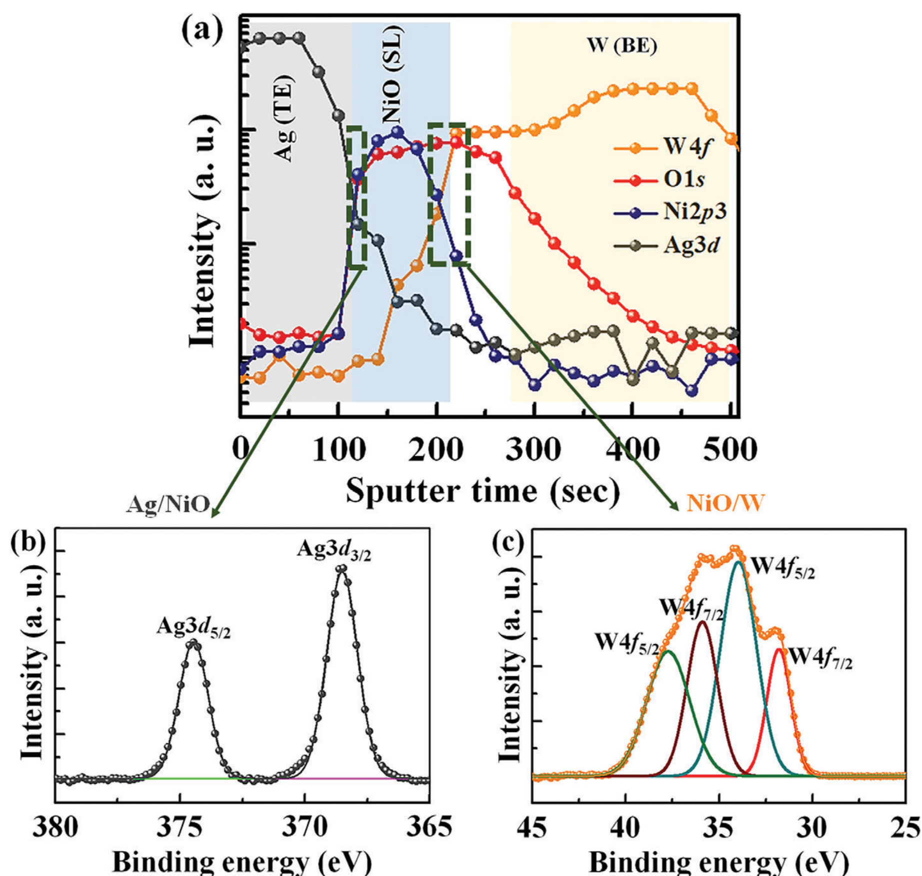

Figure 6. a) XPS depth profile of the fabricated Ag/NiO/W stack at 1 keV Ar^+ plasma, b) XPS core/valence spectra of Ag/NiO interface, and c) XPS core/valence spectra of NiO/W interface.

Further, a comparison has been made with the most recent works on CF-based ReRAM devices, taking into consideration their architecture incorporating oxidizable electrodes and/or NiO SL as presented in **Table 1**, in order to further assert the fabricated Ag/NiO/W ReRAM device structures as a potential candidate for the highly durable and reliable, multi-storage nonvolatile memory applications. The comparison suggests that the current work, that is, fabricated Ag/NiO/W ReRAM structures, shows a better trade-off between operating voltages, resistance ratio, and endurance cycle. Additionally, it eliminates the dependence on forming voltage and inherits the characteristics of the multi-level states.

3. Conclusion

In summary, we have successfully demonstrated highly stable, reliable, and voltage-controlled multi-level ReRAM device architecture of Ag/NiO/W structures. The ReRAM structures

Table 1. Comparison of this work with previously reported metal oxide SL and/or oxidizable electrode-based ReRAM devices.

Structure	V_F	V_S/V_R	RR	Cycles	Level	Ref.
$Ag/SiO_2/TiN$	FF	0.5/−0.5	10^4	10^6	S	[49]
$Cu/SiO_2/TiN$	FF	0.5/−0.5	7×10^2	10^5	S	[49]
ITO/ZnSnOy/ZnSnOx/ITO	FF	1/−1	10^2	10^8	S	[45]
TiN/HfN/ZrN/TiN	FF	0.8/−0.6	NA	10^7	S	[62]
Ag/NiO/ZnO/ITO	FF	5/−3	$\approx 10^4$	≈50	S	[17]
$Ag/TiO_X/n^+$-Si	FF	4/−4	10^5	150	M	[48]
$Al/Ag_2Se/Pt$	FF	0.13/−0.2	$\approx 10^3$	10^2	S	[63]
Ag/ZnO/TiN	3	1.5/−1	10	$\approx 10^3$	S	[64]
Ag/NiO/W	FF	0.93/−1	≈52, $\approx 10^2$, and $\approx 10^3$	$\approx 10^4$	M	This work

V_F: forming voltage; FF: forming free; V_S/V_R: SET/RESET voltage; *RR*: resistance ratio; S: Single level switching; M: Multilevel switching.

© 2024 The Authors. Advanced Electronic Materials published by Wiley-VCH GmbH

exhibited multi-level storage controlled by modulating negative voltages and also showed distinctive yet stable voltage-controlled resistance states up to 10^4 cycles owing to the WO_y interlayer formed at the NiO/W interface. The fabricated Ag/NiO/W ReRAM presents three levels of distinct states of operation by switching the device from HRS to LRS or vice-versa by modulating the voltage pulse schemes. The resistive switching behavior of the fabricated Ag/NiO/W structures showed that the devices can attain LRS and HRS at minimum voltage up to 1 and −1 V, respectively, and the mechanism comprehensively elucidated the Schottky barrier height modulation with respect to the variation in polarity of the DC sweep voltages along with metallic filament model which decreases the switching voltage. The proposed switching mechanism also describes the role of the induced WO_y interface layer at NiO/W in suppressing the redundant growth of Ag filament at BE and hence the confined CF formed in the proximity of BE results in low statistical variations while switching between states (HRS and LRS) corresponds to the significant endurance and retention characteristics. The analog switching behavior and multiple resistance states showed by Ag/NiO/W proved its candidacy for high-density, scalable future non-volatile memory applications.

4. Experimental Section

The nickel oxide (NiO) precursor solution was prepared by the facile sol–gel method[13,40] (more details are provided in Section S1, Supporting Information).

Supporting Information

Supporting Information is available from the Wiley Online Library or from the author.

Acknowledgements

The authors acknowledge the Centre for Design and Fabrication of Electronic Devices (C4DFED); Class 100 cleanroom facility, Indian Institute of Technology (IIT) Mandi, India, for sample preparation, as well as electrical characterization facilities, and FESEM facility for nano-scale cross-section imaging.

Conflict of Interest

The authors declare no conflict of interest.

Data Availability Statement

The data that support the findings of this study are available in the supplementary material of this article.

Keywords

analog resistive switching, electrochemical metallization, memristor, multi-level switching, pseudo ternary phase

Received: October 17, 2023
Revised: December 23, 2023
Published online:

[1] Y. Chen, H. H. Li, I. Bayram, E. Eken, *IEEE Des. Test* **2017**, *34*, 8.
[2] R. Waser, R. Dittmann, G. Staikov, K. Szot, *Adv. Mater.* **2009**, *21*, 2632.
[3] D. B. Strukov, G. S. Snider, D. R. Stewart, R. S. Williams, *Nature* **2008**, *453*, 80.
[4] D. S. Jeong, R. Thomas, R. S. Katiyar, J. F. Scott, H. Kohlstedt, A. Petraru, C. S. Hwang, *Rep. Prog. Phys.* **2012**, *75*, 076502.
[5] S. Choudhary, M. Soni, S. K. Sharma, *Semicond. Sci. Technol.* **2019**, *34*, 5009.
[6] D.-H. Kwon, K. M. Kim, J. H. Jang, J. M. Jeon, M. H. Lee, G. H. Kim, X.-S. Li, G.-S. Park, B. Lee, S. Han, M. Kim, C. S. Hwang, *Nat. Nanotechnol.* **2010**, *5*, 148.
[7] Y. Yang, P. Gao, S. Gaba, T. Chang, X. Pan, W. Lu, *Nat. Commun.* **2012**, *3*, 732.
[8] Y. Yang, S. Choi, W. Lu, *Nano Lett.* **2013**, *13*, 2908.
[9] A. Sawa, *Mater. Today* **2008**, *11*, 28.
[10] E. Mikheev, B. D. Hoskins, D. B. Strukov, S. Stemmer, *Nat. Commun.* **2014**, *5*, 3990.
[11] Z. Zhang, B. Gao, Z. Fang, X. Wang, Y. Tang, J. Sohn, H.-S. P. Wong, S. S. Wong, G.-Q. Lo, *IEEE Electron Device Lett.* **2015**, *36*, 29.
[12] M. Zhao, B. Gao, J. Tang, H. Qian, H. Wu, *Appl. Phys. Rev.* **2020**, *7*, 011301.
[13] S. Balatti, S. Larentis, D. C. Gilmer, D. Ielmini, *Adv. Mater.* **2013**, *25*, 1474.
[14] S. Park, H. Kim, M. Choo, J. Noh, A. Sheri, S. Jung, K. Seo, J. Park, S. Kim, W. Lee, J. Shin, D. Lee, G. Choi, J. Woo, E. Cha, J. Jang, C. Park, M. Jeon, B. Lee, B. H. Lee, H. Hwang, in *Int. Electron Devices Meeting*, IEEE, Piscataway, NJ **2012**, pp. 10.2.1–10.2.4.
[15] Y. Li, X. Li, L. Fu, R. Chen, H. Wang, X. Gao, *IEEE Trans. Electron Devices* **2018**, *65*, 5390.
[16] V. Kannan, V. Senthilkumar, J. K. Rhee, *J. Phys. D. Appl. Phys.* **2013**, *46*, 095301.
[17] S. Kossar, R. Amiruddin, A. Rasool, *Microelectron. Eng.* **2022**, *254*, 111669.
[18] F. B. Lewis, N. H. Saunders, *J. Phys. C Solid State Phys.* **1973**, *6*, 2525.
[19] P. Taylor, *Semicond. Sci. Technol.* **2018**, *33*, 37.
[20] H. Zhang, C. Cheng, B. Huang, H. Zhang, R. Chen, Y. Huang, H. Chen, W. Pei, *J. Phys. Chem. Lett.* **2021**, *12*, 3600.
[21] T.-M. Tsai, C.-C. Lin, W.-C. Chen, C.-H. Wu, C.-C. Yang, Y.-F. Tan, P.-Y. Wu, H.-C. Huang, Y.-C. Zhang, L.-C. Sun, S.-Y. Chou, *J. Alloys Compd.* **2020**, *826*, 154126.
[22] S. Yu, Y. Wu, R. Jeyasingh, D. Kuzum, H.-S. P. Wong, *IEEE Trans. Electron Devices* **2011**, *58*, 2729.
[23] S. Gaba, P. Sheridan, J. Zhou, S. Choi, W. Lu, *Nanoscale* **2013**, *5*, 5872.
[24] D. Ielmini, H.-S. P. Wong, *Nat. Electron.* **2018**, *1*, 333.
[25] Z. Wang, S. Joshi, S. E. Savel'ev, H. Jiang, R. Midya, P. Lin, M. Hu, N. Ge, J. P. Strachan, Z. Li, Q. Wu, M. Barnell, G.-L. Li, H. L. Xin, R. S. Williams, Q. Xia, J. J. Yang, *Nat. Mater.* **2017**, *16*, 101.
[26] X. B. Yan, J. H. Zhao, S. Liu, Z. Y. Zhou, Q. Liu, J. S. Chen, X. Y. Liu, *Adv. Funct. Mater.* **2018**, *28*, 1705320.
[27] S. Biswas, A. D. Paul, P. Das, P. Tiwary, H. J. Edwards, V. R. Dhanak, I. Z. Mitrovic, R. Mahapatra, *IEEE Trans. Electron Devices* **2021**, *68*, 3787.
[28] W. Kim, S. Menzel, D. J. Wouters, Y. Guo, J. Robertson, B. Roesgen, R. Waser, V. Rana, *Nanoscale* **2016**, *8*, 17774.
[29] A. Wang, J. Zhang, G. Zha, L. Xu, W. Jie, *J. Mater. Sci. Mater. Electron.* **2021**, *32*, 10809.
[30] C. B. Lee, B. S. Kang, A. Benayad, M. J. Lee, S.-E. Ahn, K. H. Kim, G. Stefanovich, Y. Park, I. K. Yoo, *Appl. Phys. Lett.* **2008**, *93*, 042115.
[31] K. Zhang, Y. Ren, P. Ganesh, Y. Cao, *npj Comput. Mater.* **2022**, *8*, 76.
[32] A. Kindsmüller, A. Meledin, J. Mayer, R. Waser, D. J. Wouters, *Nanoscale* **2019**, *11*, 18201.

© 2024 The Authors. Advanced Electronic Materials published by Wiley-VCH GmbH

2199160x, 0, Downloaded from https://onlinelibrary.wiley.com/doi/10.1002/aelm.202300724 by Indian Institute Of Technology Mandi, Wiley Online Library on [22/01/2024]. See the Terms and Conditions (https://onlinelibrary.wiley.com/terms-and-conditions) on Wiley Online Library for rules of use; OA articles are governed by the applicable Creative Commons License

[33] M. Son, X. Liu, S. M. Sadaf, D. Lee, S. Park, W. Lee, S. Kim, J. Park, J. Shin, S. Jung, M.-H. Ham, H. Hwang, *IEEE Electron Device Lett.* **2012**, *33*, 718.
[34] M. Arita, Y. Ohno, Y. Takahashi, *Phys. Status Solidi A* **2016**, *213*, 306.
[35] T. Nakamura, K. Homma, K. Tachibana, *Nanoscale Res. Lett.* **2013**, *8*, 76.
[36] S. Wiefels, M. Von Witzleben, M. Huttemann, U. Bottger, R. Waser, S. Menzel, *IEEE Trans. Electron Devices* **2021**, *68*, 1024.
[37] P. H. Abelson, *J. Mater. Res.* **1987**, *235*, 9.
[38] R. Beyers, *J. Appl. Phys.* **1984**, *56*, 147.
[39] D.-I. B. Rumpf, *Vet. Immunol. Immunopathol.* **1997**, *55*, 359.
[40] J. Tang, F. Yuan, X. Shen, Z. Wang, M. Rao, Y. He, Y. Sun, X. Li, W. Zhang, Y. Li, B. Gao, H. Qian, G. Bi, S. Song, J. J. Yang, H. Wu, *Adv. Mater.* **2019**, *31*, 1902761.
[41] J. Bai, W. Xie, W. Zhang, Z. Yin, S. Wei, D. Qu, Y. Li, F. Qin, D. Zhou, D. Wang, *Appl. Surf. Sci.* **2022**, *600*, 154084.
[42] S. K. Mohanty, P. K. Reddy, O. K. Prasad, C.-H. Wu, K.-M. Chang, J.-C. Lin, *IEEE Electron Device Lett.* **2021**, *42*, 1770.
[43] S. Ge, Y. Wang, Z. Xiang, Y. Cui, *ACS Appl. Mater. Interfaces* **2018**, *10*, 24620.
[44] K. Vishwakarma, R. Kishore, A. Datta, *IEEE Trans. Device Mater. Reliab.* **2021**, *21*, 587.
[45] D. Kumar, A. Saleem, L. B. Keong, A. Singh, Y. H. Wang, T.-Y. Tseng, *IEEE Electron Device Lett.* **2022**, *43*, 1211.
[46] D. Sakellaropoulos, P. Bousoulas, C. Papakonstantinopoulos, S. Kitsios, D. Tsoukalas, *IEEE Electron Device Lett.* **2020**, *41*, 1013.
[47] D. A. Neamen, Semiconductor Physics and Devices: basic principles Third Edition, **2003**.
[48] U. Ag, C. Bridges, C. Hsu, P. Long, Y. Lin, *IEEE Trans. Electron Devices* **2021**, *68*, 95.
[49] D. Sakellaropoulos, P. Bousoulas, C. Papakonstantinopoulos, S. Kitsios, D. Tsoukalas, *IEEE Trans. Electron Devices* **2021**, *68*, 1598.
[50] H. Abdy, A. Aletayeb, M. Kolahdouz, E. A. Soleimani, *AIP Adv.* **2019**, *9*, 015216.
[51] J. Park, K. P. Biju, S. Jung, W. Lee, J. Lee, S. Kim, S. Park, J. Shin, H. Hwang, *IEEE Electron Device Lett.* **2011**, *32*, 476.
[52] R. Islam, G. Chen, P. Ramesh, J. Suh, N. Fuchigami, D. Lee, K. A. Littau, K. Weiner, R. T. Collins, K. C. Saraswat, *ACS Appl. Mater. Interfaces* **2017**, *9*, 17201.
[53] S. Averine, Y. C. Chan, Y. L. Lam, *2000 Int. Semiconducting and Insulating Materials Conf.*, IEEE, Piscataway, NJ **2000**, pp. 345–348.
[54] A. Mondal, S. Nandi, M. K. Yadav, A. Nandi, A. Bag, *IEEE Trans. Nanotechnol.* **2022**, *21*, 320.
[55] P. Salunkhe, D. Kekuda, *J. Mater. Sci. Mater. Electron.* **2022**, *33*, 21060.
[56] S. Science, *Semicond. Sci. Technol. Pap.* **2021**, *36*, 065006.
[57] X. Y. Qiu, R. X. Wang, Z. Zhang, M. L. Wei, H. Ji, Y. Chai, F. C. Zhou, J. Y. Dai, T. Zhang, L. T. Li, X. S. Meng, *Appl. Phys. Lett.* **2017**, *111*, 142103.
[58] G. Zhou, L. Xiao, S. Zhang, B. Wu, X. Liu, A. Zhou, *J. Alloys Compd.* **2017**, *722*, 753.
[59] S. Z. Rahaman, S. Maikap, W. S. Chen, H. Y. Lee, F. T. Chen, T. C. Tien, M. J. Tsai, *J. Appl. Phys.* **2012**, *111*, 063710.
[60] R. Sharma, A. Dhillon, D. Kumar, *Sci. Rep.* **2018**, *8*, 5189.
[61] L. Ottaviano, F. Bussolotti, L. Lozzi, M. Passacantando, S. La Rosa, S. Santucci, *Thin Solid Films* **2003**, *436*, 9.
[62] D. Kumar, U. Chand, L. W. Siang, T.-Y. Tseng, *IEEE Electron Device Lett.* **2020**, *41*, 705.
[63] K.-H. Nam, J.-H. Kim, W.-J. Cho, H.-B. Chung, *Appl. Phys. Lett.* **2013**, *102*, 192106.
[64] J. Park, H. Ryu, S. Kim, *Sci. Rep.* **2021**, *11*, 16601.

© 2024 The Authors. Advanced Electronic Materials published by Wiley-VCH GmbH

2199160x, 0, Downloaded from https://onlinelibrary.wiley.com/doi/10.1002/aelm.202300724 by Indian Institute Of Technology Mandi, Wiley Online Library on [22/01/2024]. See the Terms and Conditions (https://onlinelibrary.wiley.com/terms-and-conditions) on Wiley Online Library for rules of use; OA articles are governed by the applicable Creative Commons License